

Phys. Rev. Lett. **35**, 1076 (1975).

<sup>11</sup>C. L. Tang, J. Appl. Phys. **37**, 3945 (1959).

<sup>12</sup>D. R. Speck and W. W. Simmons, Bull. Am. Phys.

Soc. **21**, 1173 (1976).

<sup>13</sup>S. R. Gunn, Lawrence Livermore Laboratory Report No. UCID 17308, 1976 (unpublished).

## Interaction of 1.06- $\mu\text{m}$ Laser Radiation with Planar Targets

R. A. Haas, H. D. Shay, W. L. Kruer, M. J. Boyle, D. W. Phillion, F. Rainer, V. C. Rupert, and H. N. Kornblum

*University of California Lawrence Livermore Laboratory, Livermore, California 94550*

(Received 11 January 1977)

Parylene and tungsten-glass disks have been irradiated with a 1.06- $\mu\text{m}$  laser at fluxes of  $10^{13}$ – $10^{15}$  W/cm<sup>2</sup>. Analysis of the experimental results indicates that the laser-plasma interaction was characterized by critical surface steepening, rippling and/or filamentation, polarization-dependent scattering, and efficient generation of superthermal electrons. These effects were significantly stronger in the tungsten-glass experiments.

Extensive experimental studies<sup>1</sup> of the interaction of laser radiation with low  $\bar{Z}$  ( $\leq 3.5$ ) targets, covering a wide range of intensities ( $I_i \geq 10^{12}$  W/cm<sup>2</sup>) and wavelengths ( $\leq 10.6$   $\mu\text{m}$ ), indicate that the interaction process is generally strongly influenced by collective plasma processes. This Letter presents the results of 1.06- $\mu\text{m}$  laser-irradiation experiments<sup>2</sup> with the Cyclops laser<sup>3</sup> in which  $\bar{Z}$  was varied significantly by using disk targets of Parylene (C<sub>8</sub>H<sub>8</sub>) and W glass (0.75 W<sub>2</sub>O, 0.25 P<sub>2</sub>O<sub>5</sub>). Detailed measurements of the scattered laser light and x-ray and charged-particle emission characteristics show strong evidence that the interaction process was dominated by critical surface steepening, rippling and/or filamentation, polarization-dependent scattering, and efficient generation of superthermal electrons. Furthermore, the strongest noncollisional behavior occurred in the high- $\bar{Z}$  W-glass irradiations. Analysis suggests that the observed behavior of the two target types can be unified by the parameter  $\eta = V_o/V_T$ , the ratio of the electron oscillatory and thermal velocities.

The planar (650–950  $\mu\text{m}$  diam  $\times$  7  $\mu\text{m}$  thick) disks were located  $\sim 10^3$   $\mu\text{m}$  inside the focal waist in the near field of an  $f/2.5$  aspheric lens. The flux level ( $10^{13}$ – $10^{15}$  W/cm<sup>2</sup>) was varied by changing the laser pulse length (150–400 ps) and energy (5–75 J). Target damage due to amplified spontaneous emission and prepulses was found to be unimportant. An extensive array of diagnostics<sup>1,2</sup> observed laser and plasma behavior during each experiment. The time-integrated laser energy distribution in the target plane was measured during each experiment with an equivalent-lens-multiple-image camera system. The focused laser

beam, 250–300  $\mu\text{m}$  FWHM (full width at half-maximum) in diameter, exhibited a ring structure, rising (50–100%) above the central minimum. Small-scale fluctuations, 30–40  $\mu\text{m}$  in diameter and (30–50%) in relative  $I_i$ , were superimposed on these gross features.

Figure 1 shows the measured absorption  $\eta_a$  vs  $I_i$ . Both target types absorbed comparable fractions. For the  $\sim 200$ -ps experiments,  $\eta_a$  for W glass (Parylene) varied from  $\sim 38\%$  ( $\sim 30\%$ ) at  $5 \times 10^{13}$  W/cm<sup>2</sup> to  $\sim 30\%$  ( $\sim 25\%$ ) at  $5 \times 10^{14}$  W/cm<sup>2</sup>. The discrepancy between the photodiode and box calorimeter measurements should be taken as indicative of the accuracy of the energy balance

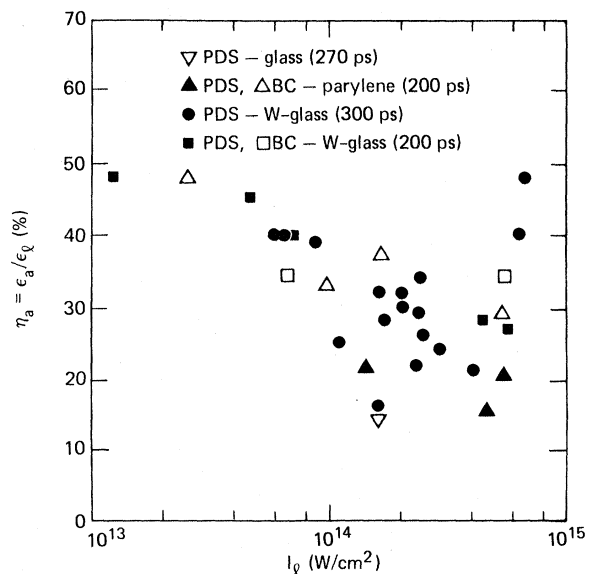


FIG. 1. Fractional laser-light absorption measurements: photodiodes (PDS) and "box" calorimeter (BC).

measurements, although the box calorimeter is expected to be more accurate since it subtended  $0.92(4\pi)$  sr around the target. The laser-light absorption fraction was also inferred by using several ion calorimeters surrounding the target. These calorimeters measured the emitted x-ray radiation and asymptotic convective energy of the plasma. They gave results that agreed, to within experimental uncertainties, with the optical energy balance measurements. For instance, in a specific W-glass irradiation experiment, at  $5.7 \times 10^{14}$  W/cm<sup>2</sup>, 28% absorption was inferred by the ion/x-ray calorimetry and 27% by photodiode measurements. On a comparable experiment, at  $5.5 \times 10^{14}$  W/cm<sup>2</sup>, 34% absorption was measured by the box calorimeter. The x-ray and ionic contributions to the calorimetry data were deconvolved with the aid of ion angular distributions deduced from Faraday detector data and x-ray angular distributions measured with pinhole cameras and x-ray microscopes. The x-ray emission at energies  $\geq 100$  eV was much larger for W glass than for Parylene; at  $10^{14}$  W/cm<sup>2</sup> it was  $0.5\epsilon_a$  for W glass and  $(0.01-0.1)\epsilon_a$  for Parylene.

The scattered laser energy distributions in and perpendicular to the incident-laser-light polarization plane exhibited several characteristics indicative of collective processes. These distributions, Fig. 2(a), for both target types were similar and strongly peaked in the backscatter direction. For  $\theta \sim 135^\circ-150^\circ$  strong azimuthal non-uniformities were observed, i. e.,  $p_\perp/p_\parallel \sim 3-4$ . A substantial fraction of the scattered laser light appeared in the plane perpendicular to the plane of polarization of the incident laser light. In Fig.

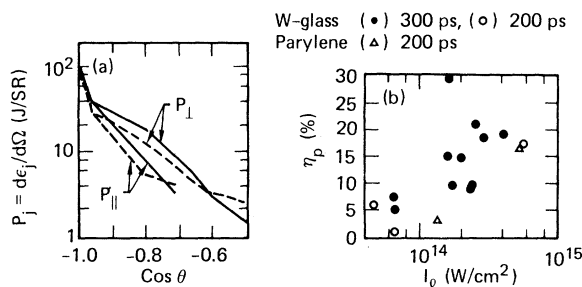


FIG. 2. (a) Laser energy scattered per unit solid angle into  $p_\parallel$  and perpendicular to  $p_\perp$  the incident laser light polarization plane as a function of the scattering angle for solid line, W glass ( $5.7 \times 10^{14}$  W/cm<sup>2</sup>, 181 ps, 27% absorption) and dashed line, Parylene ( $5.3 \times 10^{14}$  W/cm<sup>2</sup>, 195 ps, 23% absorption). (b) Fraction of the incident laser energy scattered azimuthally non-uniformly.

2(b) the fraction of the incident laser energy scattered azimuthally nonuniformly  $\eta_p = \int (p_\perp - p_\parallel) d\Omega / \epsilon_i$  is plotted as a function of  $I_i$ . This quantity increases with  $I_i$  as  $\eta_a$  is decreasing, is relatively insensitive to target composition, and is greater for the long-pulse-length experiments.

Simple theoretical estimates and LASNEX<sup>1,2,4</sup> simulations without ponderomotive force show that at  $10^{14}$  W/cm<sup>2</sup> the W-glass target plasmas would be stripped to a  $\bar{Z}$  of 13-15 and absorb  $\sim 70\%$  of the incident laser energy by inverse bremsstrahlung (IB), about twice the  $\eta_a$  for Parylene targets. The data show a much lower  $\eta_a$  for the high- $Z$  targets and little distinction in scattering characteristics between the Parylene and W-glass disks. Since most of the IB occurs quite close to critical density  $n_c$ , it is strongly reduced by density profile steepening due to ponderomotive forces at  $n_c$  and competition with Brillouin scattering. The azimuthally nonuniform scattering could result from resonant absorption on a steepened, rippled, critical surface or Brillouin sidescatter. The estimated threshold for sidescatter in these experiments is  $10^{14}$  W/cm<sup>2</sup>. For a steepened density profile, Brillouin sidescatter occurs most strongly at  $(0.5-0.7)n_c$ . As observed, the azimuthally scattered light then refracts out of the plasma at  $\theta \sim 135^\circ-150^\circ$ . Sidescatter is expected to be more important in these experiments than previous ones<sup>1</sup> due to the larger focal spots and longer pulse lengths. Furthermore, at these intensities, induced scatter does not readily self-limit by modification of the plasma density.

Local steepening of the density profile near  $n_c$  is consistent with polarimetry measurements.<sup>5</sup> In these experiments the average degree of linear polarization,  $p$ , of the scattered laser light at  $\theta = 164^\circ$ ,  $\varphi = 45^\circ$  was measured to be 0.92 relative to the direction of polarization expected if the plasma reflected laser light as a perfectly conducting plane. According to detailed calculations,<sup>5</sup> this value of  $p$  corresponds to a scale length of  $\leq 4 \mu\text{m}$  for a plane wave incidence angle of  $8^\circ$ . The depolarization contributions due to the finite angular extent of the beam, plasma turbulence, critical surface steepening or breakup, and Faraday rotation were estimated<sup>5</sup> using a reference polarimeter in the plane of polarization,  $\varphi = 0^\circ$ , of the incident laser beam.

Figure 3 shows evidence of filamentation initiated by a nonuniform laser beam. Similar, but less pronounced, behavior was also observed for Parylene. The position of x-ray hot spots cor-



FIG. 3. X-ray micrograph,  $\bar{E}_\nu \approx 2.5$  keV, taken at a  $45^\circ$  angle from the front surface of a W-glass target at  $5.7 \times 10^{14}$  W/cm $^2$ . The bar denotes 100  $\mu$ m.

relates with hot spots on the incident beam. However, the appearance of the x-ray hot spots only at  $\geq 10^{14}$  W/cm $^2$  does not correlate with the observation that the laser beam profile contained similar hot spots at all  $I_l$  examined. In the figure each nonuniformity (hot spot) is surrounded by a less intense ring. The outer dimension of each ring or halo compares closely to the initial FWHM of the corresponding hot spot on the laser beam. The estimated filamentation  $e$ -folding length for the conditions of Fig. 3 is 12  $\mu$ m for a 20  $\mu$ m diam inhomogeneity at  $0.5n_c$ . Thus the halo is possibly a consequence of filamentation collapse and conduction inhibition by self-generated magnetic fields. For example, a thermoelectrically generated solenoidal field  $B \sim \tau_L \theta_e / L_n L_\theta \sim 0.8$  MG about each hot spot when  $\tau_L \sim 200$  ps,  $L_n \sim 20$   $\mu$ m, and  $L_\theta \sim 40$   $\mu$ m constrains the electron diffusion time across it to 220 ps.

The x-ray emission spectra plotted in Fig. 4 show further evidence of collective laser plasma interactions. Above 4–5 keV the typical x-ray spectrum consisted of two parts each having a roughly exponential behavior; a low energy ( $\leq 10$  keV) component due to line radiation and the tails of photorecombination edges and a high energy component due to bremsstrahlung from energetic, nonthermal electrons. Figure 4 shows the  $I_l$  dependence of the normalized x-ray intensity at 30 keV, and the effective "temperature",  $\theta_h$ , of the high-energy x rays. Both quantities increase with  $I_l$  indicating an increase in plasma coronal temperature. Furthermore, at a given intensity  $f_\nu$  and  $\theta_h$  are largest for the W-glass experiments. For equal fast electron distributions 5 times as many hard x rays should be observed for W glass as for Parylene. Instead, the hard x-ray spectra from W-glass irradiations are 30–40 times more intense than those from comparable Parylene experiments. These results indicate that at a given  $I_l$  heated electron distributions were harder in the W-glass experiments. Also, typically 4–5 times as much energy in emit-

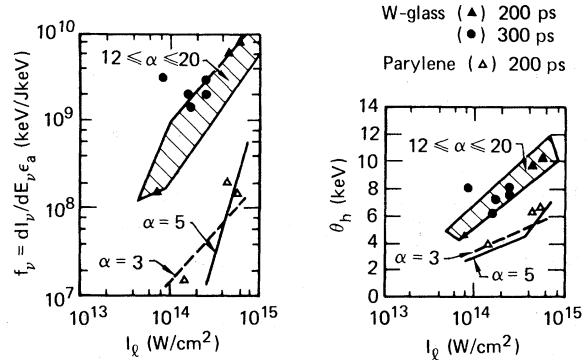


FIG. 4. X-ray spectral emission characteristics delineated according to target and pulse length. The LASNEX calculations constrained absorption to occur at  $n_c$  and heating exclusively into superthermal electrons for W glass, cross-hatched region, and for Parylene with (dashed line), without (solid line) the Fried-Gould inhibition (Ref. 1) to electron conduction.  $\theta_h$  is computed on the 10 to 30 keV interval.

ted fast electrons ( $\geq 30$  keV) was detected in W-glass irradiations as in Parylene.

In LASNEX, laser-light absorption via collective processes produces nonthermal electrons according to the source function  $\dot{n}_s(v) = C_e v^2 \times \exp(-mv^2/2\alpha\theta_e)$  where  $\theta_e$  is the mean electron temperature and  $\alpha$  is a parameter. The results of LASNEX simulations are shown in Fig. 4. In the W-glass calculations, matching the intensity and slope of the hard x-ray emission required, for the measured  $\eta_a$ , that all the absorbed laser energy go into fast electrons with  $\alpha = 10$ –20. For Parylene, the assumption that a major fraction of  $\epsilon_a$  produces hot electrons with  $\alpha \sim 3$ –5 was required to reproduce the data. Thus the calculations suggest strong collective absorption in all cases and that relatively much hotter electrons are generated in the W-glass experiments.

Simulations and theory $^6$  indicate that  $\eta$  is an important parameter characterizing laser-plasma interactions. As a consequence of the high radiative efficiency of the W-glass plasmas, their  $\theta_e$  (300–400 eV based on comparison of low energy x-ray spectra with LASNEX simulations $^2$ ) was  $\sim 2.5$  times less than corresponding Parylene plasmas. Thus  $\eta$  was larger by a factor of  $\sim 1.5$  in the W-glass experiments than in the Parylene irradiations. The absorption, scattering, and x-ray spatial emission characteristics discussed earlier are certainly consistent with this difference. The parameter  $\eta$  may also be the common denominator for the superthermal elec-

tron heating distributions. A plot of  $\alpha\theta_e$  vs  $\eta$  for the set of all LASNEX simulations reproducing the hard x-ray data is roughly a single curve. Closer inspection of Fig. 4 reveals that the Parylene curves are generated by shifting the W-glass curves up a factor of 3–4 in laser intensity. This shift is just that required to achieve comparable values of  $\eta$ . This interpretation implies that the hot-electron temperature increases as the background plasma temperature decreases, a behavior that has not been predicted theoretically.<sup>7,8</sup> However, plasma simulations<sup>8</sup> do show an increase in hot-electron temperature for higher  $\bar{Z}$  materials, since heated electrons are then scattered more often back into the heating region.

The authors especially thank H. Ahlstrom, C. Hendricks, J. Holzrichter, K. Manes, and J. Nuckolls for encouragement and support and K. Estabrook, R. Lerche, L. Koppel, L. Richards, V. Slivinsky, and G. Zimmerman for valuable contributions and discussions.

This work was performed under the auspices of the U. S. Energy Research and Development Administration under Contract No. W-7405-Eng-48.

<sup>1</sup>B. H. Ripin, *Appl. Phys. Lett.* **30**, 134 (1977); B. H. Ripin *et al.*, *Phys. Rev. Lett.* **34**, 1313 (1975); R. Sigel *et al.*, *Phys. Rev. Lett.* **36**, 1369 (1976); S. Jackel *et al.*, *Phys. Rev. Lett.* **37**, 95 (1975); D. V. Giovanelli *et al.*, *J. Appl. Phys.* **47**, 2907 (1976); C. Yamanaka *et al.*, *Phys. Rev. A* **6**, 2335 (1972); R. A. Haas *et al.*, *Phys. Fluids* **20**, 338 (1977), and *J. Appl. Phys.* **47**, 1318 (1976).

<sup>2</sup>H. D. Shay *et al.*, University of California Report No. UCRL-79438 (to be published).

<sup>3</sup>J. Glaze, *Opt. Eng.* **15**, 136 (1976).

<sup>4</sup>G. B. Zimmerman, University of California Report No. UCRL-74811, 1973 (unpublished).

<sup>5</sup>D. W. Phillion *et al.*, University of California Report No. UCRL-78444 (to be published).

<sup>6</sup>K. G. Estabrook, E. J. Valeo, and W. L. Kruer, *Phys. Fluids* **18**, 1151 (1975); D. W. Forslund, J. M. Kindel, Kenneth Lee, and E. L. Lindman, *Phys. Rev. Lett.* **36**, 35 (1976); C. S. Liu, Marshall N. Rosenbluth, and Roscoe B. White, *Phys. Fluids* **17**, 1211 (1974); P. Kaw, G. Schmidt, and T. Wilcox, *Phys. Fluids* **16**, 1522 (1973).

<sup>7</sup>D. W. Forslund *et al.*, *Phys. Rev. Lett.* **39**, 284 (1977).

<sup>8</sup>K. G. Estabrook and W. L. Kruer, University of California Report No. UCRL-79617, 1977 (unpublished).

## Transport of Long-Mean-Free-Path Electrons in Laser-Fusion Plasmas

J. R. Albritton, I. B. Bernstein,<sup>(a)</sup> E. J. Valeo,<sup>(b)</sup> and E. A. Williams  
*Laboratory for Laser Energetics, University of Rochester, Rochester, New York 14623*  
(Received 29 August 1977)

The Fokker-Planck kinetic equation for suprathermal electrons which are confined in a spherical plasma by the sheath potential and collide with colder denser electrons and ions is investigated. In the region where the collisional mean free path,  $\lambda$ , is longer than the spatial scale length,  $L$ , the kinetic equation is reduced by averaging it along an orbit between reflections by the sheath. The electrons are seen to diffuse in impact parameter relative to the plasma core while slowing down in velocity. The resulting heat flow scales as  $(L/\lambda)n_{\text{sth}}mv_{\text{sth}}^3$ .

A complete theory of transport processes in inertially confined plasmas is not yet available. This has led to the adoption of *ad hoc* strong flux limiting schemes to replicate certain observations in laser-fusion experiments.<sup>1</sup> Several anomalous mechanisms have been investigated in support of this treatment, such as enhanced turbulence or magnetic fields.<sup>2,3</sup> In the high-intensity regime of interest, however, collisionless absorption of incident energy results in the production of highly energetic electrons.<sup>4</sup> Here we discuss a systematic treatment which considers in detail the "neoclassical" transport problem, i.e., that associated with these long-mean-free-path electrons suffering only Coulomb collisions. A new, nonlocal transport description emerges

naturally which is distinctly different in spirit from the local description implied by flux limiting. We find that the energy flux into the plasma is only a small fraction of the (half-space) free-streaming value. It is important to understand the complete classical description quantitatively in order to identify accurately the nature and the degree of significant anomaly, if any, which remains to be explained.

The problem is complicated by the fact that the plasma parameters vary over a wide range depending on position in the target and time during the driving pulse. For that part of the electron distribution with scattering and energy-relaxation mean free paths,  $\lambda_{90}$  and  $\lambda_e$ , both small compared to the background gradient scale length  $L$ ,



FIG. 3. X-ray micrograph,  $\bar{E}_\nu \approx 2.5$  keV, taken at a  $45^\circ$  angle from the front surface of a W-glass target at  $5.7 \times 10^{14}$  W/cm<sup>2</sup>. The bar denotes 100  $\mu$ m.